Seventh International Conference on CFD in the Minerals and Process Industries
CSIRO, Melbourne, Australia
9-11 December 2009

2D SIMULATIONS OF INTERFACIAL INSTABILITIES AT DEFORMABLE SINGLE DROPLETS

Kathrin BÄUMLER[1], Mirco WEGENER[2], Eberhard BÄNSCH[1], Anja PASCHEDAG[3]

[1] FAU Erlangen Nürnberg, Institute of Applied Mathematics III, 91058 Erlangen, Germany
[2] TU Berlin, Department of Chemical Engineering, 13355 Berlin, Germany
[3]University of Applied Science Berlin, 13353 Berlin, Germany

ABSTRACT

In liquid/liquid extraction processes, e.g. in ternary systems, where the transfer of a solute between a dispersed and a continuous phase is considered, reliable predictions of mass transfer coefficients and retention times are indispensable. Especially in the case, where interfacial instabilities like drop deformation and Marangoni-convection occur, the influencing factors and their quantitative nature are not yet fully understood.

In our numerical model we consider a Newtonian viscous two phase flow, representing a single deformable drop. Simulations are performed using the academic code NAVIER, which features a sharp interface model and a variational formulation of the curvature. This approach provides an effective method for a consistent, very exact description of discrete surface stresses.

Results of drop rise velocities and mass transfer rates in the 2D case of spherical as well as deformable drops are presented (diameters varying from 1 *mm* to 5 *mm)*.

The simulations are compared to experimental results in the system water/toluene and to numerical results of non-deformable drops obtained by STAR-CD. Especially with the onset of drop deformation, the system is excellently reflected by the simulations, i.e. the terminal velocities calculated with NAVIER show a deviation of no more than 4% to the experimental results.

NOMENCLATURE

A_d	reference area	$[m^2]$
c	concentration	$[mol/m^3]$
C_D	drag coefficient	$[-]$
d_p	diameter of drop	$[m]$
D	diffusion coefficient	$[m^2/s]$
I	identity matrix	$[-]$
F_A / F_D	buoyancy/drag force	$[N]$
g	gravity constant	$[m/s^2]$
H	partition coefficient	$[-]$
m	mass of drop	$[kg]$
p	pressure	$[N/m^2]$
Pe	Peclet number	$[-]$
Re	Reynolds number	$[-]$
t	time	$[s]$
u / u_∞	velocity/ terminal velocity	$[m/s]$
U	velocity scale	$[m/s]$
x_{bc}	barycenter of drop	$[m]$
$\dot{x}_{bc} / \ddot{x}_{bc}$	velocity/acceleration at x_{bc}	$[m/s]$
γ_0	interfacial tension	$[N/m]$
Γ	interface of drop	$[-]$
κ	mean curvature	$[1/m]$
ν	outer unit normal on surface	$[-]$
ρ	density	$[kg/m^3]$
μ	dynamic viscosity	$[kg/ms]$
Ω	domain	$[-]$
σ	Newtonian stress tensor	$[N/m^2]$

Subscripts

c/d	continuous/ dispersed phase

INTRODUCTION

Liquid/liquid extraction processes play an important rôle in the process industries. In industrial applications knowledge of small scale behaviour of single drops can be used to improve the design of extraction columns.
Thus the complex mechanisms that dominate retention times, terminal velocities, and mass transfer rates of single drops are an area of active research, both experimentally and numerically.

The direct numerical simulation of single drops in a continuous liquid phase with mass transfer and a deformable interface is a challenging task. Due to steep gradients and nonlinear interactions the interface in particular has to be resolved with sufficient accuracy. There are several possible methods of tracking the location of a deformable interface:

One approach is the widely used VoF (Volume of Fluid) method (Hirt & Nichols, 1981; Bothe, 2005; Davidson & Rudman, 2002). In this approach an additional time-dependent transport equation for the volume fraction of the dispersed phase is solved. The level-set method (Osher & Sethian, 1988; Wang et al., 2008; Bertakis et al., 2008) is another successful and popular method of obtaining an implicit representation of the interface.

These implicit methods have the advantage of being able to capture drop coalescence or breakup, as they can deal with topological changes. However, if applicable, mesh moving or front tracking methods have the potential to be

much more accurate (Bänsch, 2002; Tryggvason et al., 2002; Dijkhuizen et al., 2005).

In a finite-element mesh-moving method the interface always coincides with an (interior) boundary of the underlying mesh and is thus perfectly aligned. Since the triangulation is deformed in each time step, mesh distortion has to be avoided by appropriate grid smoothing.

The key ingredient for a feasible and highly effective mesh-moving method for the present problem is to work in a co-moving frame of reference (Maxey & Riley, 1983; Wang et al., 2008). The interfacial conditions are implemented using a **S**ubspace **P**rojection **M**ethod (SPM) (Bänsch & Bäumler, 2009).

The numerical results are compared to simulation results of spherical drops using the commercial code STAR-CD, and with experimental data from the system water/toluene (Wegener et al., 2007).

The aim of this paper is to gain further insight into interfacial phenomena like drop deformation, and in future studies of Marangoni effects, and study their influence on mass transport.

MODEL DESCRIPTION OF 2 PHASE FLOW

We split the continuous and dispersed phase into $\Omega = \Omega_c \cup \Omega_d$. The interface Γ is given as $\Gamma = \overline{\Omega_c} \cap \overline{\Omega_d}$, compare Figure 1.

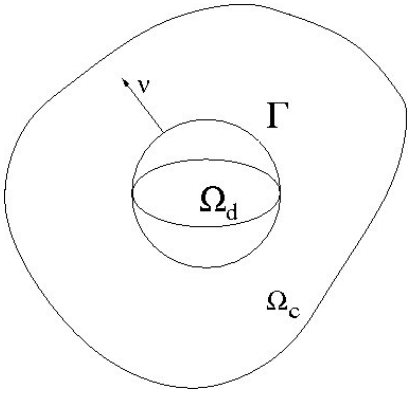

Figure 1: Indication of domain.

Fluid Dynamics and mass transport in bulk phase

We assume the following restrictions on the fluids:

- incompressible, Newtonian fluids,
- mutually immiscible fluids,
- constant temperature,
- rotational symmetric flow,
- constant parameters.

For simplification of the mass transfer, we assume:

- no reaction of solute and the bulk phases,
- negligible mass of solute,
- no breakup or coalescence of drops,
- no Marangoni effects.

Under these assumptions, the governing equations of the two phase flow in the bulk phases are the incompressible Navier-Stokes equations with a Newtonian stress tensor: $\sigma_i = \mu_i(\nabla \mathbf{u}_i + \nabla \mathbf{u}_i^T) - pI$ in Ω_i.

$$\nabla \cdot \mathbf{u}_i = 0, \quad in\ \Omega_i \tag{1}$$

$$\frac{\partial \rho_i \mathbf{u}_i}{\partial t} + \rho_i(\mathbf{u}_i \cdot \nabla)\mathbf{u}_i - \nabla \cdot \sigma_i = \rho_i g \ in \Omega_i \tag{2}$$

The mass transport is described by a convection-diffusion equation in each phase.

$$\frac{\partial c_i}{\partial t} + (\mathbf{u}_i \cdot \nabla)c_i - D_i \Delta c_i = 0, \quad in \Omega_i \tag{3}$$

The subscript $i \in \{c, d\}$ indicates the respective phase.

(1) to (3) are subject to appropriate initial conditions.

Interface conditions

For further information on fluid mechanics and mass transfer at interfaces we refer to Deen, 1998, and Clift et al., 1978.

We introduce the notation

$$[f] = \lim_{\substack{x \to x_0 \\ x \in \Omega_c}} f(x) - \lim_{\substack{x \to x_0 \\ x \in \Omega_d}} f(x)$$

for a jump of a quantity (scalar or vector valued) across the interface.

Fluid dynamics

Due to the ***no-slip*** condition the tangential velocities are continuous across the interface. Moreover, since we consider no bulk flow across the interface, the normal components are also continuous.

With the above notation the no-slip condition reads:

$$[u] = 0. \tag{4}$$

The stress balance at the interface is given for every point on the interface by:

$$[\sigma \cdot \nu] = \gamma_0 \kappa \nu - \nabla_S \gamma(c). \tag{5}$$

Here, κ denotes the mean curvature of the interface, γ_0 is the interfacial tension of the pure system (without added solute). ∇_S denotes the surface gradient (the projection of the gradient on the tangential plane).

In neglecting Marangoni-convection, equation (5) simplifies to

$$[\sigma \cdot \nu] = \gamma_0 \kappa \nu \tag{5*}$$

In the simplified equation (5*) there is no back coupling of solute concentration to the velocity field. Thus the fluid field can be solved independently of the concentration.

Mass transfer

Assuming Fick's law, the conservation of mass leads to the balance relation at the interface:

$$[\partial_\nu (Dc)] = 0, \tag{6}$$

and using Henry's law we get

$$\frac{c_d}{c_c} = H, \tag{7}$$

with the partition coefficient H depending on the involved fluids.

Force balance

The force balance of the drop is given by Newton's second law, see equation (8), and Figure 2.

$$m \ddot{x}_{bc} = F_A + F_D \tag{8}$$

Here F_A is the buoyancy force, given by:

$F_A = m(1 - \frac{\rho_d}{\rho_c})g$, and F_D is the drag force due to the flow field given by $F_D = -\int \sigma_c \cdot \nu \, dS$.

NUMERICAL METHOD IN NAVIER

Simulations of spherical and deformable drops have been realized with the academic code NAVIER. This code consists of a finite-element scheme with the ability of free-surface treatment (Bänsch, 1998, 2001).

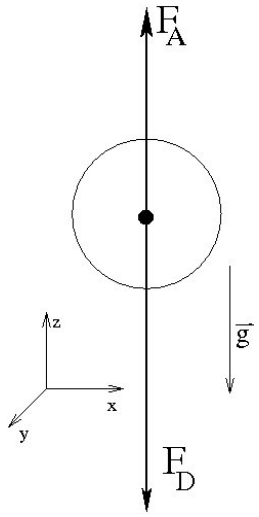

Figure 3: Schematic diagram of forces

For time discretization, a fractional-step-theta scheme (Bristeau et al., 1987) in a variant as operator splitting is used and the Taylor-Hood finite-element for space discretization. For a correct calculation of the flow field and thus of rise velocities, grid independence has to be assured. Grid dependency tests have been carried out for the setting of a rigid droplet. These tests were performed on different triangulations, varying in size and refinement level. Finally a triangulation was chosen, with a distance of 7 radii from drop surface to the wall, consisting of 1300 triangles, which inherits a relative error of less than 1% with respect to the terminal velocity.

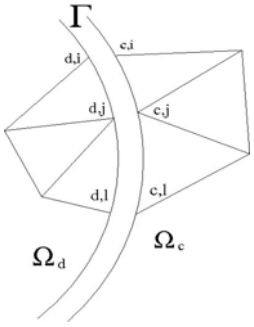

Figure 2: Virtual node doubling.

Interface handling in NAVIER

The crucial part of a two-phase flow implementation is the interface representation. As mentioned in the introduction, we use a mesh-moving method. The handling of the discontinuities of pressure and concentration is delicate and essential for the resulting accuracy of the overall method.

This problem is solved within NAVIER by a (virtual) doubling of the interface nodes. Introducing parent and child nodes on the interface, there are two associated nodes of the finite element space c_j and d_j (see Figure 3, note that in the figure the interface Γ is pulled apart for better visualisation).

Since deformations of the interface are caused only by normal velocities, the location of the new interface can be calculated by solely considering the normal component of the velocity, using the kinematic condition:

$$U_\Gamma = (u \cdot \nu)u, \quad on\, \Gamma .$$

As mentioned in the introduction, the interfacial equations (4) and (7) are realized via a special **S**ubspace **P**rojection **M**ethod (SPM) (Bänsch & Bäumler, 2009).

SPM operates directly on the nodal basis of the finite element representation. It consists of a local projection, operating on interface nodes only. It is thus easy to implement as well as computationally efficient. The momentum flux condition (5*) is implemented by variational curvature treatment. Flux condition (6) is a natural boundary condition in our formulation.

Moving Reference Frame

As mentioned above, the equations are solved in a moving reference frame. The reference frame is moved according to the position of the barycenter of the drop. This method allows us to compute the solutions in a significantly smaller computational domain and, even more importantly, to use a mesh moving method without facing severe mesh distortion.

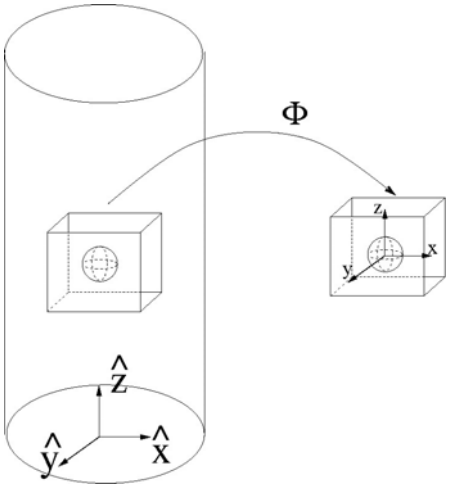

Figure 4: Schematic diagram of the transformation.

If not stated otherwise, in the following, we denote by $\hat{x}$ the coordinates in the reference frame relative to a fixed observer.

We use a coordinate transformation Φ on the coordinates $\hat{x}$ that keep the barycenter of the moving drop in the center of the transformed coordinate system x for all times.

$$\Phi(\hat{x}_{bc}) = 0$$

This transformation is given for a known position of the barycenter of the drop by:

$$\Phi : (\hat{x}; t) \to (x; t)$$

$$\Phi(\hat{x}; t) = \hat{x} - x_{bc} .$$

Note that the coordinates of the barycenter of the drop are a function of time.

With the given transformation Φ, we define functions u, p, c in the moving reference frame.

$$u_i(x;t) := \hat{u}_i(\hat{x};t) - \dot{x}_{bc}\,(t)$$

$$p_i(x;t) = \hat{p}_i(\hat{x};t) + \rho_c\, \ddot{x}_{bc}(t) \cdot x\,(t)$$

$$c_i(x;t) = \hat{c}_i(\hat{x};t) .$$

Note that the function p is chosen to be dependent on ρ_c in both fluid phases.

These modified velocity and pressure fields yield again a Navier-Stokes like equation. One difference is an additional acceleration term, analogous to a volume force on the right hand side of the Navier-Stokes equations for the dispersed phase. Another consequence of this transformation is the occurrence of modified boundary conditions.

The new defined concentration c fulfils a diffusion-convection equation as in (3) in each phase.

Nondimensionalization

We obtain the following dimensionless groups by nondimensionalization.

- Reynolds number $\mathrm{Re}_i := \frac{U d_p \rho_c}{\mu_i}$
- Peclet number $Pe_i := \frac{U d_p}{D_i}$

Note that these numbers are discontinuous over the phase boundary.

Determining the acceleration

The acceleration in each time step is computed via the force balance (8), which in turn depends on the drag force. Thus, the pressure $\hat{p}$ of the reference coordinate system is needed, which can be obtained from the modified pressure p by subtracting a gradient field corresponding to the transformation Φ.

Stabilization of convection-dominated flow

In finite-element simulations convection—dominated flows may lead to numerical instabilities, since the solution tends to oscillate at sharp fronts. These sharp fronts occur in the current setting at the interface of the droplet, where the data is discontinuous. Therefore a stabilization technique (the streamline diffusion method) was implemented (Johnson, 1995). Nevertheless the simulations reveal that further stabilization is necessary for a reliable prediction of mass transport in flows with higher Peclet numbers. In the future another method, shock capturing (Johnson, 1995), will be used additionally.

RESULTS

The results that we obtain in our simulations with the academic code NAVIER are validated with numerical results using the commercial software STAR-CD in 3D-simulations, as well as with data obtained in experiments.

25°	ρ[kg/m³]	D [m²/s]	μ[kg/ms]	γ[N/m]	H [-]
water	998.2	1.140E-7	1.0E-3	3.5E-2	0.63
toluene	866.7	2.900E-7	0.586E-3		

Table 1: Material properties.

In Table 1 material parameters for the ternary system water/toluene/acetone at 25°C are given. The diffusion coefficients are chosen two orders of magnitude higher than in reality. This simplification is assumed, since the mass transfer is a strongly convection-dominated problem (see above). However, we expect this modified setting to give first insights into the effects of drop deformation on mass transport of the original setting. The Peclet number considered for the calculations is of the order $Pe_c \approx 10^3$. Therefore the simulations already reflect a convection dominated regime, and discussions by Clift et al. (1978) suggest only a quantitative change, considering the effect of shape change. Nevertheless future simulations with $Pe_c \approx 10^5$, using a shock capturing method, are currently prepared. For all data presented in this paper, material properties are chosen according to Table 1. Water is considered to be the continuous phase and acetone the transferring solute from the dispersed phase to the continuous phase.

	Navier deform	Experiments Wegener et al. (2008)	Navier spherical	STAR-CD spherical Wegener et al. (2008)	Hamielec et al. (1963)
d_p in mm	terminal velocity [m/s]				
1	0.0412	0.0402	0.0412	0.0384	0.0406
1.5	0.0731	0.0705	0.0731	0.0680	0.0710
2	0.1124	0.1112	0.1129	0.1051	0.1057
2.5	0.1542	0.1544	0.1607	0.1505	0.1438
2.7	0.1678				
3.0	0.1790	0.1833	0.2160	0.2039	0.1850
3.2	0.1810				
3.5	0.1780	0.1840	0.2750	0.2586	0.2289
4.0	0.1758	0.1798	0.3732	0.3138	0.2752
4.5	0.1700	0.1751	0.4607		0.3239
5		0.1740	0.5567		0.3746

Table 2: Terminal velocities of deformable and spherical drops in the setting water/toluene.

Velocity

Since STAR-CD is limited to the case of spherical drops, we compare simulations of NAVIER of spherical drops (third column in Table 2) with 3D-simulations in STAR-CD (fourth column in Table 2) and analytical results from Hamielec et al. (1963) (fifth column in Table 2) for the spherical case. The deviation of terminal velocities calculated with NAVIER to STAR-CD is less than 7% except for the 4 mm drop, where the deviation rises to 16%. In comparison with results from Hamielec et al. our results show a growing deviation with increasing drop diameter, up to 33% for a 5 mm drop.

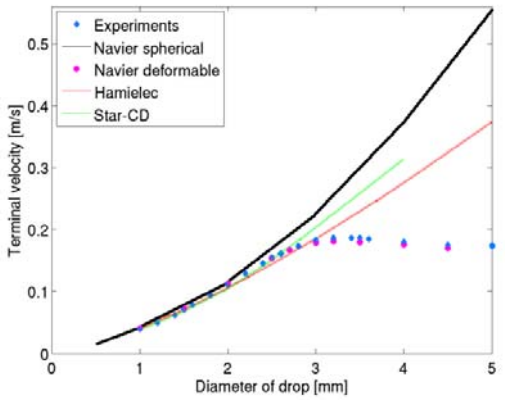

Figure 5: Terminal velocities of rising deformable and spherical toluene drops in water for varying diameter.

Results of NAVIER simulating deformable drops (first column in Table 2) are then compared to experiments (second column in Table 2). The agreement is excellent, since the comparison reveals a deviation of no more than 3.5%. Since the terminal velocity of the 4.5mm drop is periodic in time (see Figure 7), we have calculated a mean

velocity over one period to determine the terminal velocity.

In comparison to deformable drops, the higher terminal velocity of spherical drops is clearly reproduced in the simulations with NAVIER (see Figure 3).

The simulations reflect the fact that deformable drops reach a maximum of terminal velocity at a diameter of about 3.2 mm to 3.5mm. With increasing diameter, there is no further increase of terminal velocities in simulations after 3.2mm, or experiments after 3.5mm. This can be observed in the simulation, presented in Figure 5.

The change of shape regime from spherical to ellipsoidal drop shape is reproduced in the simulations, as shown in Figure 6. As stated by Clift et al., 1978, this onset of deformation starts at a diameter of approximately 3mm. In Figure 6, the interface of the simulated drops is printed at three different times. It is possible to validate that a drop with a diameter of 2mm still keeps its spherical shape, whereas a drop with diameter 3mm is already slightly ellipsoidally shaped. The larger the diameter, the more pronounced the ellipsoidal shape.

At a diameter of 4.5mm the drops in the simulations start to wobble. This wobbling of the shape leads to a periodic change of the terminal velocity (see Figure 7).

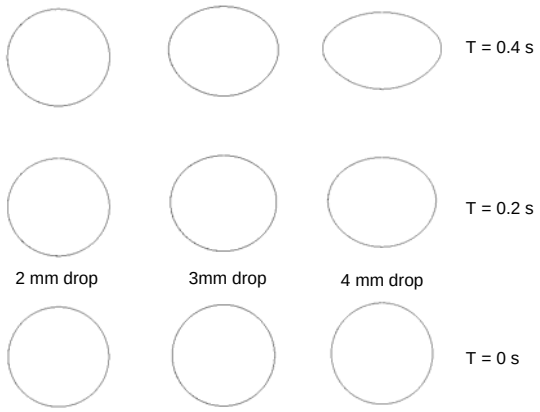

Figure 6: Shape of deformable drops at different times t = 0s; t=0.2s;t=0.4s; simulations with NAVIER.

Mass transfer

Mass transfer simulations for deformable and spherical drops have been performed. In Figure 8 isolines of concentration are plotted for spherical and deformable simulations of drops with a diameter varying from 2 mm to 4mm. It can be observed that the shape of the isolines transforms, in the case of deformable drops, to a more circular torus, whereas in the case of spherical drops, naturally the shape remains more elliptic. The relative position of the maximum of concentration to axial drop diameter does not change significantly however, neither for varying drop diameters, nor in comparing spherical to deformable drops.

Transient results of the dimensionless mean concentration $c^* := \bar{c}/c_0$ are plotted in Figure 9. $\bar{c}$ is the mean concentration in the droplet, and c_0 is the initial solute concentration. No significant distinction can be made between runs of deformable and spherical drops.

According to the lower rise velocity and the convection dominance of the concentration equation the drops with smaller diameter show a slower descent of mean concentration. For illustration of the convection dominance of the problem, Figure 10 shows the streamlines of the velocity field and the concentration.

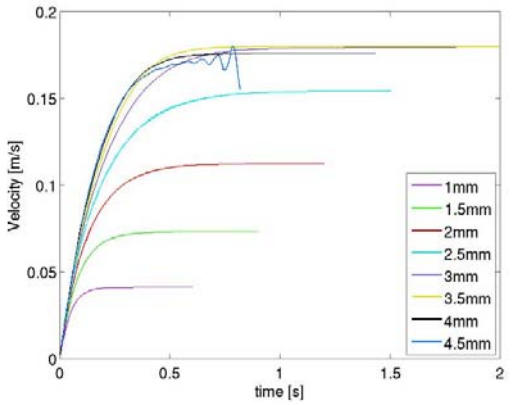

Figure 7: Transient rise velocities for different drop diameters in the system water/toluene for deformable drops.

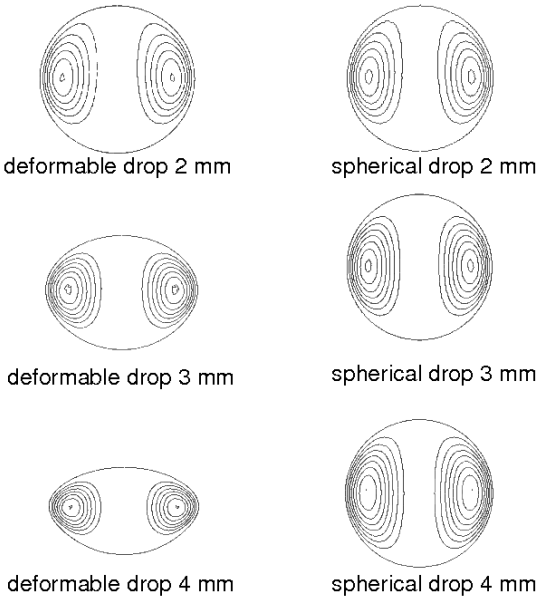

Figure 8: Isolines of concentration and shape of drops. Left column shows deformable drops, right column shows spherical drops.

CONCLUSION AND OUTLOOK

In the present paper, simulations of transient rise velocities and mass transfer for single spherical as well as deformable drops for varying diameters have been performed with the academic code NAVIER.

Regarding onset of deformation and terminal rise velocity, the results are in very good agreement with experimental data. Furthermore, there is also good agreement of non-deformable, spherical drops at least for small diameters. For larger drop diameters, 3D effects are no longer negligible, so that our 2D results deviate by up to 16% and 33%, respectively, compared to results from the commercial code STAR-CD, and with analytic results, using the drag correlation of Hamielec et al. (1963).

Thus, further investigations (i.e. 3D-simulations with NAVIER) are required for better results.

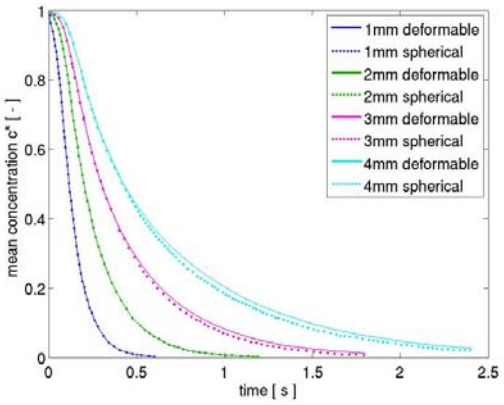

Figure 9. Transient mean concentration for different drop diameters and spherical and deformable runs

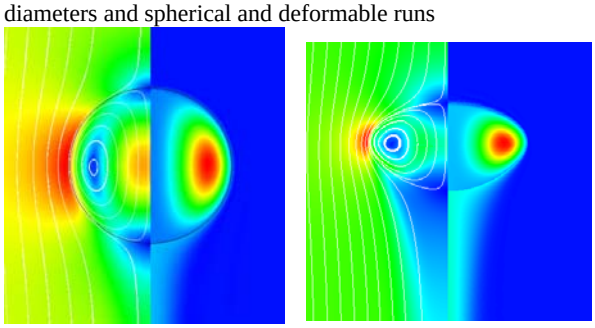

Figure 10: Spherical (left) and deformable (right) drop of 4mm diameter; concentration and velocity magnitude with streamlines. Simulations performed with NAVIER.

The significant role of drop deformation on the velocity is excellently represented in NAVIER. This could be shown by comparison to experimental data, obtained in the pure system water/toluene.

Also changes in drop shapes show a good analogy to data presented by Clift et al. (1978). The simulations reveal that despite the significant differences of velocity regimes in deformable and spherical cases, the influence on mass transport due to drop deformation is negligible in our setting.

However, when it comes to mass transport, we still face numerical instabilities due to the strong convection-dominated character of the problem. We are currently working with stabilization techniques in order to be able to model the concentration effectively. A consequent next step is the research on systems with Marangoni-convection.

ACKNOLEDGEMENT

The authors would like to acknowledge the German Research Foundation (DFG) for financial support under Grant BA 1727/6-01 and Grant Pa1009/2-01.

REFERENCES

BÄNSCH, E: (1998),"Numerical methods for the instationary Navier-Stokes equations with a free capillary surface", *Habilitation Thesis*

BÄNSCH, E: (2001),"Finite element discretization of the Navier-Stokes equations with a free capillary surface", *Nume. Math* , **88**, 203-235

BÄNSCH, E: , BÄUMLER, K.,"Numerical methods for single drop flow", *in preparation*

BRISTEAU, M., GLOWINSKI, R., PERIAUX, J.: (1987),"Numerical Methods for the Navier-Stokes equations. Applications to the simulation of compressible and incompressible viscous flows", *Computer Physics Reports*, **6**, 73-187

DAVIDSON, M., RUDMAN, M: (2002),"Volume –of-Fluid calculation of heat or mass transfer across deforming interfaces in two-fluid flow", *Numerical heat transfer: Part B*, **41**, 291-308

DEEN, W. (1998), "Analysis of transport phenomena", *Oxford University Press*, New York

BERTAKIS, E., GROß, S., GRANDE, J., FORTMEIER, O., REUSKEN, A., PFENNIG, A, (2008), "Validated simulation of droplet sedimentation with finite-element and level-set methods" *(submitted to Elsevier*, December 23, 2008)

D. BOTHE: "VOF-Simulation of fluid particle dynamics" *In Proc. 11th Workshop on two-phase flow predictions* (M. Sommerfeld, ed.), Merseburg, April 2005

CLIFT, R., GRACE, J. and WEBER, M. (1978) "Bubbles, Drops and Particles", *Academic Press, London*

DIJKHUIZEN, W. VAN SINT ANNALAND, M. and KUIPERS, H (2005), "Numerical investigation of closures for interface forces in dispersed flows unsing a front tracking model", *Fourth International Conference in the Oil and Gas, metallurgical & Process Industries SINTEF / NTNU*, Trondheim, Norway, June 6-8 2005

HAMIELEC, A.E., STOREY, S.H., WHITEHEAD, J.M. (1963). "Viscous flow around fluid spheres at intermediate Reynolds-numbers" *Canadian Journal of Chemical Engineering*, **12**, *246-251*

HIRT, C., NICHOLS, B. (1981),"Volume of fluid (VOF) Method for the dynamics of free boundaries", *Journal of Computational Physics*, **39,***201-225*

JOHNSON, C. (1995),"Numerical solution of partial differential equations by the finite element method", *Cambridge University press*

MAXEY, M., RILEY, J. (1983),"Equations of motion for a small rigid sphere in a nonuniform flow", *Phys. Fluids*, **26(4),** *883-889*

OSHER, S., SETHIAN, J., (1988) "Fronts propagating with curvature-dependent speed: algorithm based on Hamilton-Jacobi formulations, *Journal of Computational Physics*, **79,***12-49*

TRYGGVASON, G., BUNNER, B., ESMAEELI, A., JURIC, D., AL-RAWAHI, N., TAUBER, W., HAN,J., NAS, S., JAN. Y. -J., (2001), "A Front-Tracking method for the Computations of multiphase flow", *Journal of Computational Physics*, **169(2)**, 708-759

WANG, J., LU, P., WANG, Z., YANG, C., MAO, Z., (2008), "Numerical simulation of unsteady mass transfer by the level set method", *Chemical Engineering Science*, **63**, 3141-3151

WEGENER, M., GRÜNIG, J., STÜBER, J. PASCHEDAG, A.R., KRAUME, M. , (2007), "Transient rise velocity and mass transfer of a single drop with interfacial instabilities – experimental investigations", *Chemical Engineering Science*, **62**, 2967-2978

WEGENER, M.; KRAUME, M.; PASCHEDAG, A.R.: "Terminal and transient drop rise velocity of single toluene droplets in water", (2009, corrected proof) *AIChE Journal, DOI 10.1002/aic.11969*